

Numerical Study of Aerodynamic Flutter Derivatives for a Plate Girder Bridge Deck

Jong-Dae Kim^{*1a}

¹ Samsung C&T Corporation, Seocho, Seoul 137-956, Korea

Abstract. Computational fluid dynamics (CFD) technique has been used to estimate flutter derivatives of a plate girder bridge. Similar to the forced oscillation wind tunnel tests, CFD simulations employed moving mesh technique with prescribed heaving and rotational deck motions. Flutter derivatives obtained from CFD simulations are compared with wind tunnel test results and shows good agreements. This study presents that CFD approach can be employed to assess the aerodynamic stability of plate girder long-span bridges.

Keywords: flutter derivatives; plate girder bridge, moving mesh technique.

1. Introduction

The development of new construction materials and design technologies has spawned a generation of structurally efficient long-span bridges. And these light and flexible structures pose a special challenge to structural engineers. Due to their low damping and low natural frequencies, long-span bridges are very vulnerable to wind load and the dynamic amplification of the fluctuating wind load may cause collapse of bridges. To prevent this catastrophic disaster, aerodynamic stability should be assessed during the design stage. For several decades, wind tunnel tests have been the most reliable and commonly used tools for aerodynamic stability estimation of long-span bridges.

To estimate aerodynamic behavior of long-span bridges, Scanlan (1996) proposed a relation of wind loads and their induced structural motions. The wind loads are expressed as linear combinations of aerodynamic parameters, called flutter derivatives.

Flutter derivatives can be extracted from wind tunnel tests of bridge section models. Basically there are two approaches, free oscillation and forced oscillation techniques. Free oscillation test has limitations in high wind speed region in the case that aerodynamic damping is high. Forced oscillation test is more complicated and difficult to perform but results are more reliable in high wind speed region. Details of wind tunnel test techniques and associated issues, refer works done by King et. al. (2004)

This study adopted numerical approach called CFD (computational fluid dynamics) technique to calculate flutter derivatives. Similar to forced oscillation wind tunnel test, 2-dimensional model of the plate girder deck employing moving mesh technique is used to simulate the flow field around oscillating deck. Turbulent flow induced forces are measured and flutter derivatives are extracted from the relations between force coefficients and girder motions.

2. Forced Oscillation Technique

Eq. 1 is proposed by Scanlan (1996) to explain the relation of wind loads and corresponding structural motions. Since the number of unknowns, i.e., flutter derivatives (H^* and A^*) are 8 while there are only two equations (Eq. 1a for heaving and Eq. 1b for torsional motion). To solve this system of equations, unknowns are eliminated by fixing motions. Using this approach, total 4 types of tests or simulations are carried out as follows;

Case 1, lift motion (fix rotation) and lift force measurement

Case 2, lift motion (fix rotation) torsional moment measurement

Case 3, torsional motion (fix heaving) and torsional moment measurement

Case 4, torsional motion (fix heaving) and lift force measurement

^{*a} Principal Researcher, Corresponding author, E-mail: jd2009.kim@samsung.com

Since the flutter derivatives are a function of reduced velocity, numerical simulations have been performed from low to high reduced velocities. Reduced velocity is controlled by adjust motion frequency or wind speeds.

$$m_h(\ddot{h} + 2\zeta_h \omega_h \dot{h} + \omega_h^2 h) = L \quad (1.a)$$

$$m_\alpha(\ddot{\alpha} + 2\zeta_\alpha \omega_\alpha \dot{\alpha} + \omega_\alpha^2 \alpha) = M \quad (1.b)$$

$$L = \frac{1}{2} \rho U^2 B [KH_1^* \dot{h}/U + KH_2^* B \dot{\alpha}/U + K^2 H_3^* \alpha + K^2 H_4^* h/B] \quad (1.c)$$

$$M = \frac{1}{2} \rho U^2 B^2 [KA_1^* \dot{h}/U + KA_2^* B \dot{\alpha}/U + K^2 A_3^* \alpha + K^2 A_4^* h/B] \quad (1.d)$$

, where L , M are the Lift and Moment produced by the moving deck, ρ is the air density, B is the deck width, K is a reduced frequency ($B\omega/U$) or reciprocal of reduced velocity V_r , U is the wind speed at deck height, ω is the circular natural frequency, and H_{1-4}^* and A_{1-4}^* are the lift and torsion flutter derivatives.

2.1 Case 1: Lift Motion - Lift Force Measurement (Fix Rotation)

As a special case, rotational motion is limited and only vertical or heaving motion is allowed. Eliminating unknowns associated with rotational motion, Eq. 1 is simplified to Eq. 2.

$$L = \frac{1}{2} \rho U^2 B [KH_1^* \dot{h}/U + K^2 H_4^* h/B] \quad (2.a)$$

$$\frac{L}{\frac{1}{2} \rho U^2 B} = C_L = [2KH_1^* \dot{h}/U + 2K^2 H_4^* h/B] \quad (2.b)$$

Assuming the deck motion is harmonic ($h(t) = h_o \theta^{i\omega t}$), heaving motion can be written using complex functions:

$$\dot{h} = \frac{\ddot{h}}{i\omega} = -\frac{i\ddot{h}}{\omega} \quad (3.a)$$

$$h = \frac{-i}{\omega} \dot{h} = \frac{-i-i}{\omega} \frac{\ddot{h}}{\omega} = -\frac{\ddot{h}}{\omega^2} \quad (3.b)$$

Substitute Eq.3 into Eq.2, the measured lift force and vertical acceleration can be expressed in terms of aerodynamic derivatives as shown in Eq. 4.

$$\begin{aligned} C_L &= [2(B\omega/U) * H_1^* (-i\dot{h}/\omega)/U + 2(B\omega/U) * (B\omega/U) * H_4^* (-\ddot{h}/\omega^2)/B] \\ &= (\ddot{h} * 2B/U^2) [H_1^* (-i) + H_4^* (-)] \end{aligned} \quad (4.a)$$

$$\frac{C_L}{\ddot{h}} \frac{U^2}{2B} = [-iH_1^* - H_4^*] \quad (4.b)$$

$$H_1^*(K) = \frac{C_L}{\ddot{h}} \left[-\frac{iU^2}{2B} \right] \quad (4.c)$$

$$H_4^*(K) = \frac{C_L}{\dot{h}} \left[-\frac{U^2}{2B} \right] \quad (4.d)$$

2.2 Case 2: Lift Motion -Torsional Moment Measurement (Fix Rotation)

Similar to Case 1, rotational motion is limited and only vertical or heaving motion is allowed. Eliminating unknowns associated with rotational motion, Eq. 1 is simplified to Eq. 5.

$$M = \frac{1}{2} \rho U^2 (B^2) \left[KA_1^* \dot{h} / U + K^2 A_4^* h / B \right] \quad (5.a)$$

$$\frac{M}{\frac{1}{2} \rho U^2 (B^2)} = C_M = \left[KA_1^* \dot{h} / U + K^2 A_4^* h / B \right] \quad (5.b)$$

Substitute Eq.5 into Eq.2, the measured torsional moment and vertical acceleration can be expressed in terms of aerodynamic derivatives as shown in Eq. 6.

$$\frac{C_M U^2}{\dot{h} B^2} = -iA_1^* - A_4^* \quad (6.a)$$

$$A_1^*(K) = \frac{C_M}{\dot{h}} \left[-\frac{iU^2}{B} \right] \quad (6.b)$$

$$A_4^*(K) = \frac{C_M}{\dot{h}} \left[-\frac{U^2}{B} \right] \quad (6.c)$$

2.3 Case 3: Torsional Motion - Torsional Moment Measurement (Fix Heaving)

As a special case, heaving motion is limited and only torsional motion is allowed. Eliminating unknowns associated with heaving motion, Eq. 1 is simplified to Eq. 7.

$$M = \frac{1}{2} \rho U^2 (B^2) \left[KA_2^* B \dot{\alpha} / U + K^2 A_3^* \alpha \right] \quad (7.a)$$

$$\frac{M}{\frac{1}{2} \rho U^2 (B^2)} = C_M = \left[KA_2^* B \dot{\alpha} / U + K^2 A_3^* \alpha \right] \quad (7.b)$$

Substitute Eq.7 into Eq.2, the measured torsional moment and rotational acceleration can be expressed in terms of aerodynamic derivatives as shown in Eq. 8.

$$\frac{C_M U^2}{\ddot{\alpha} B^2} = -iA_2^* - A_3^* \quad (8.a)$$

$$A_2^*(K) = \frac{C_M}{\ddot{\alpha}} \left[-\frac{iU^2}{B^2} \right] \quad (8.b)$$

$$A_3^*(K) = \frac{C_M}{\ddot{\alpha}} \left[-\frac{U^2}{B^2} \right] \quad (8.c)$$

2.4 Case 4: Torsional Motion - Lift Force Measurement (Fix Heaving)

Similar to Case 3, heaving motion is limited and only rotational is allowed. Eliminating unknowns associated with heaving motion, Eq. 1 is simplified to Eq. 9.

$$L = \frac{1}{2} \rho U^2 (B) [KH_2^* B \dot{\alpha} / U + K^2 H_3^* \alpha] \quad (9.a)$$

$$\frac{L}{\frac{1}{2} \rho U^2 (B)} = C_L = [KH_2^* B \dot{\alpha} / U + K^2 H_3^* \alpha] \quad (9.b)$$

Substitute Eq.9 into Eq.2, the measured lift force and rotational acceleration can be expressed in terms of aerodynamic derivatives as shown in Eq. 10.

$$\frac{C_L}{\ddot{\alpha}} \frac{U^2}{B^2} = -iH_2^* - H_3^* \quad (10.a)$$

$$H_2^*(K) = \frac{C_L}{\ddot{\alpha}} \left[-\frac{iU^2}{B^2} \right] \quad (10.b)$$

$$H_3^*(K) = \frac{C_L}{\ddot{\alpha}} \left[-\frac{U^2}{B^2} \right] \quad (10.c)$$

3. Numerical Methods

Fig.1 shows the plate girder deck and computational domain. The width and depth of the deck are B=0.4574m and H=0.048m, respectively. The size of computational domain size is Lx = 4.11m in horizontal and Ly=1.05m in vertical directions, respectively. For boundary conditions, uniform velocity with 0.3% turbulence intensity at inlet, outflow condition at outlet and symmetry boundary conditions at upper and low boundaries.

The computational domain is modeled with approximately 40,000 triangular cells. For spatial discretization, 2nd order scheme for momentum and continuity equations are used. PISO scheme is employed for pressure-velocity coupling. RNG k-e model is used to solve Reynolds averaged Navier-Stokes equations (RANS).

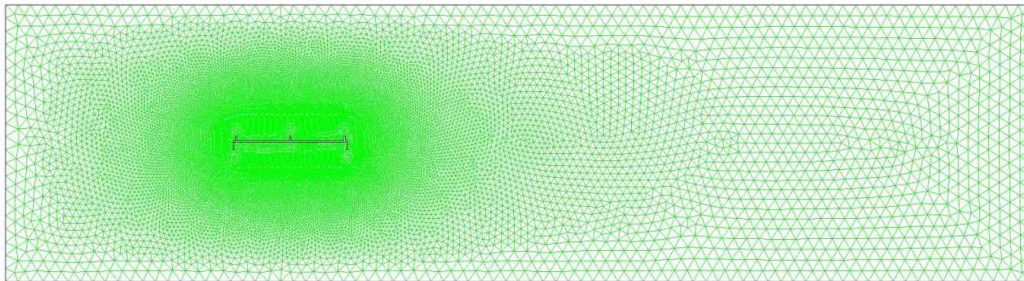


Fig. 1 Two dimensional section model and computational domain

4. Results

Fig. 2 shows snapshots of flow field around the girder in terms of vorticity contours corresponding to Case 3 or Case 4, only rotational motion is allowed. When the wind speed is low, shear layer generated from leading edges reattaches on the bridge deck and vertical structures shed along the deck surfaces (Fig.2 a and b). As wind speed increases, the reattachment position moves downward on the deck and shear layers extended beyond the trailing edge of the deck.

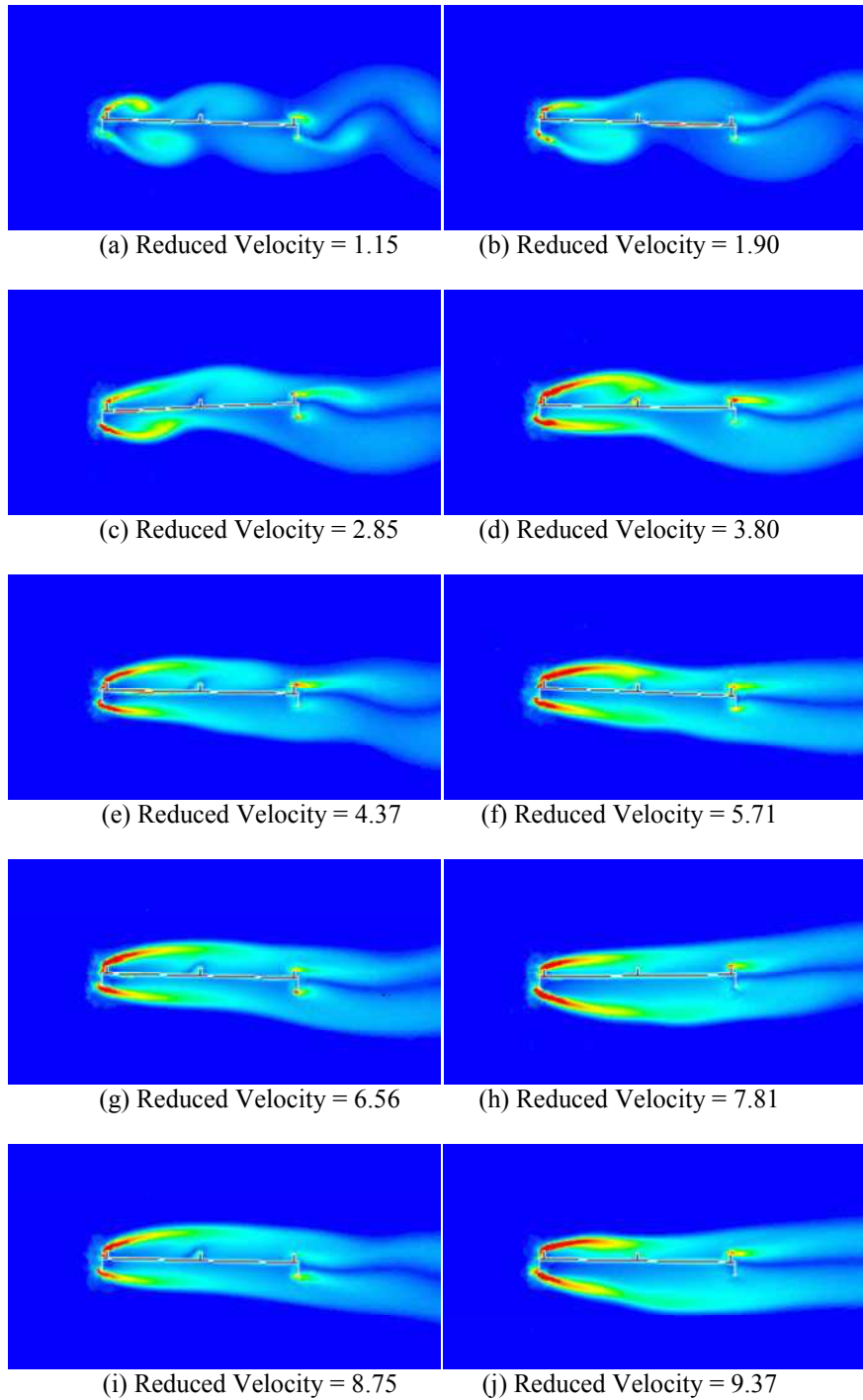


Fig. 2 Snapshot of CFD simulations: Vorticity contours

Fig. 3 presents the flutter derivatives obtained from CFD simulations and wind tunnel tests. Two results match well except $A2^*$. The discrepancy is the slope of the curve when the reduced velocity is higher than 4. During the wind tunnel tests, wind loads are calculated from the integration of pressures measured along the deck perimeter. Since there is no space for pressure measurement holes and associated pressure transferring tubes on the edge beams, wind tunnel test results are not able to include all the wind loads acting on the deck surfaces. But CFD simulation obtained wind loads measured from all deck surfaces. This difference may produce the discrepancy of $A2^*$ slope. This study shows that inclusion of wind loads on edge beam surfaces will produce slightly different aerodynamic stability characteristics for a plate girder bridge, especially on torsional flutter stability estimation.

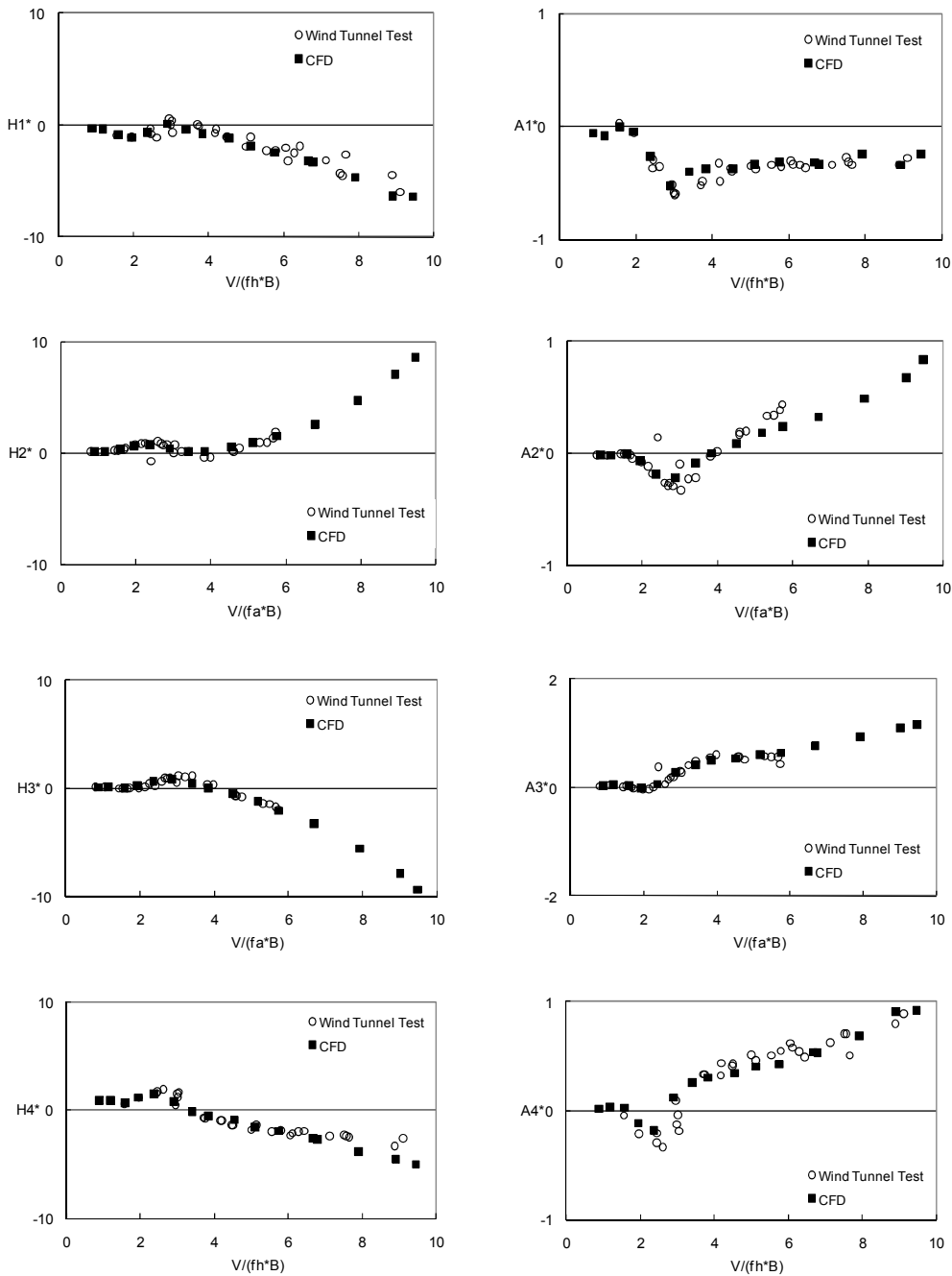


Fig. 3 Flutter derivatives of a plate girder bridge deck

5. Conclusions

Similar to forced oscillation wind tunnel tests, CFD simulations have been carried to obtain flutter derivatives for a plate girder bridge deck. Moving mesh technique is used to simulate the flow field around the vertically or rotationally oscillating deck. Turbulent flow induced forces are measured and associated flutter derivatives are extracted from the relations between force coefficients and girder motions.

Comparing flutter derivatives from CFD simulations with wind tunnel tests, two results are almost identical except A_2^* . The discrepancy comes from the difference of force measurement schemes where wind tunnel test model was not able to include wind loads acting on the edge beams.

Considering good agreement of CFD and wind tunnel test results, the author recommend CFD simulations can be applied to assess the aerodynamic stability of plate girder long-span bridges during the preliminary design stage.

References

- King, J.P.C., Kim, J.D., Hong, H.P. and Kong, L. (2004) " A Study of Wind Effects for the Stonecutters Bridge, Section Model Investigation of Aerodynamic Derivatives", The University of Western Ontario, Faculty of Engineering Research Report, BLWT-SS37-2004, The University of Western Ontario, London, Ontario, Canada, 2004.
- Simiu, E., and Scanlan, R., (1996), "Wind Effects on Structures, Fundamentals and Applications to Design", John Wiley & Sons, New York